Pulling Thin Single Crystal Silicon Wafers from a Melt: The New Leading-Edge Solar Substrate

Parthiv Daggolu[a*], Jesse Appel[a], Peter Kellerman[a], and Nathan Stoddard[a]

[a] *Leading Edge Equipment Technologies*

Wilmington, MA

Abstract

The Floating Silicon Method (FSM) has been established as a viable, stable method for growing single crystal ribbons directly from a silicon melt. With intense helium jet cooling to drive the linear progress of a [111] facet, pulled in the <110> direction, ribbons in the 0.6 – 3.0 mm thickness range can be grown at linear growth rates from 0.3 mm/s to >6 mm/s as reported in the literature. We report on recent progress towards growing (100) oriented ribbons with a net thickness of less than 200 microns and a ribbon width up to 18 cm using a stable, continuous process in the Leading Edge prototype furnace. The 3D details of the single crystal growth are explained by extending the mechanics of the Limit Cycle Theory, with novel Internal Side Effect morphology described by a proposed Facet Flow Theory. Grown-in crystalline defect distributions are described as well as values of critical impurities like oxygen, carbon, dopants, and metals that are relevant for use as wafers for solar cells.

Key words: A2. Horizontal ribbon growth, A1. Single crystal growth, A1. Growth models, A1. Interfaces, A1. Interface kinetics, A1. Roughening

* Corresponding author

Email address: daggolu@leadingedgetech.io

1. Introduction

The production of silicon wafers continues to be the most cost-, capital-, and carbon-intensive step of silicon-based solar panel manufacturing. Today, the solar industry uses the Czochralski (Cz) process that grows single-crystal silicon ingots, from large and energy intensive furnaces. These ingots are wire-sawed and chemically polished to produce the finished wafer. This process wastes over half of the silicon ingot, consumes diamond-coated wire, and constitutes over 80 percent of the panel's final carbon footprint. At Leading Edge Equipment Technologies, we use the Floating Silicon Method (FSM) technology that directly produces single-crystal ribbons that are laser cut into wafers [6]. This is accomplished without the excessive waste of wire saw and using only one-third of the energy. We project that the FSM technology enables 50% reduction in manufacturing costs, 7% 'drop-in' increase in solar panel power and 56% reduction in manufacturing emissions [2].

FSM is a type of Horizontal Ribbon Growth (HRG) [3-6] technique where heat is removed from the top surface of a molten pool to solidify a sheet that is then pulled horizontally at a constant velocity to establish a steady-state process. FSM is unique compared to the other HRG techniques by forming a stable faceted growth front that supports fast single-crystal pull rates. In addition, the floating ribbon is extended over a long length of the melt that allows for distinct thermal zones to be established, each optimized for a specific function. In this paper, we describe details of the FSM process and the phenomenology and theory of faceted layer growth at the leading edge. Further, we describe progress towards the goal of producing single crystal substrates in the form-factor needed for solar industry while enhancing the wafer quality over Cz for optimal solar cell performance.

2. FSM Process

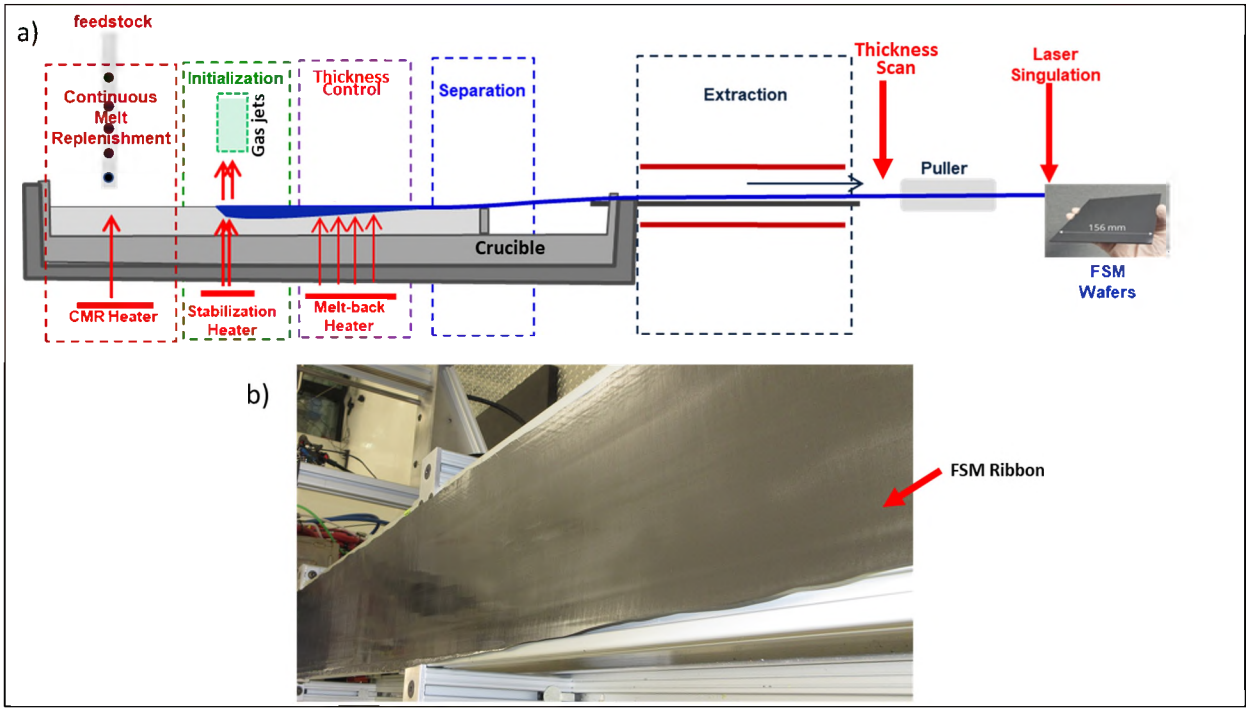

Figure 1: a) Schematic of the FSM process showing different zones. b) An example of an as-grown FSM ribbon on the puller coming out of the furnace (not shown)

To grow thin ribbons that result in the required form factor, the FSM process uses a shallow rectangular quartz tray filled with molten silicon where the floating ribbon is continuously pulled off the surface. It is this floating nature of the Si ribbon that allows for distinct zones in the FSM process, as shown in Figure 1, each independently optimized for its function in the crystallization process. The FSM process starts with inserting a seed cut from a CZ (100) wafer into the furnace, floating it on the melt, and moving it such that the leading edge of the seed is brought into the "Initialization" zone. The optimized cooling from the top and heating from the bottom provide the necessary conditions to initiate faceted growth at the same speed as the ribbon pull speed, thereby creating a steady state process. The details of the coupled physics at the leading edge, associated engineering design aspects and process characteristics are described in further detail in Section 3. Due to the faceted nature of the leading-edge growth and the nature of the gas jet cooling, the

ribbon starts out with a thickness of >1 mm and hence necessitates a means to thin down to target thickness (~180um). The floating nature of the ribbon presents the opportunity to melt back the ribbon in the "Thickness Control" zone, downstream to the Initialization Zone as shown in Figure 1. The target thickness and uniformity are achieved in this zone using controlled heating from the bottom and/or controlled cooling from the top and is discussed in greater detail in Section 4. Further downstream is the "Separation" zone where the ribbon separates from the melt at the crucible end wall by a pinned meniscus that holds the melt in and allows the ribbon to pull out "dry". The ribbon then enters the "Extraction" zone where it is cooled to ambient temperature with optimized axial/transverse thermal gradients, minimizing the buildup of any deleterious thermal stress that can affect ribbon shape and quality. Immediately after the ribbon exits the furnace, the thickness profile is scanned and fed back to a control loop that alters the heating/cooling settings in the thickness control zone. The ribbon is then cut into appropriate length sections by an in-line laser singulator, resulting in wafers ready for further solar processing. At the very upstream end of the furnace, the melt is continuously replenished by dropping polysilicon into the melt through a feed tube at a controlled rate and using a localized heater to melt it. This maintains the melt height for steady state operation.

3. Crystal Growth at the Leading Edge

One of the most striking features of FSM ribbons is the presence of "facet lines" on the top surface. These lateral lines run continuously across the ribbon with spacing of ~10 microns and depth of ~ 1um. This phenomenon was described in a previous work [1] by a 2-dimensional (2D) Limit Cycle Theory (LCT). In this paper, we explore the 3D aspects of FSM ribbon growth, account for newly described phenomena that occur at the sides of the ribbon, referred to as "side effects" (SE), and propose a Facet Flow Theory to explain how such a fast crystal growth rate can be maintained in a facetted manner. The basis for this "heuristic" theory is the phenomenology, including the ribbon

leading edge shape antimony demarcation cross-sections of the ribbon, and topography of the ribbon surface, in addition to knowledge of solidification kinetics and heat flow.

3.1. Average Cooling Flux

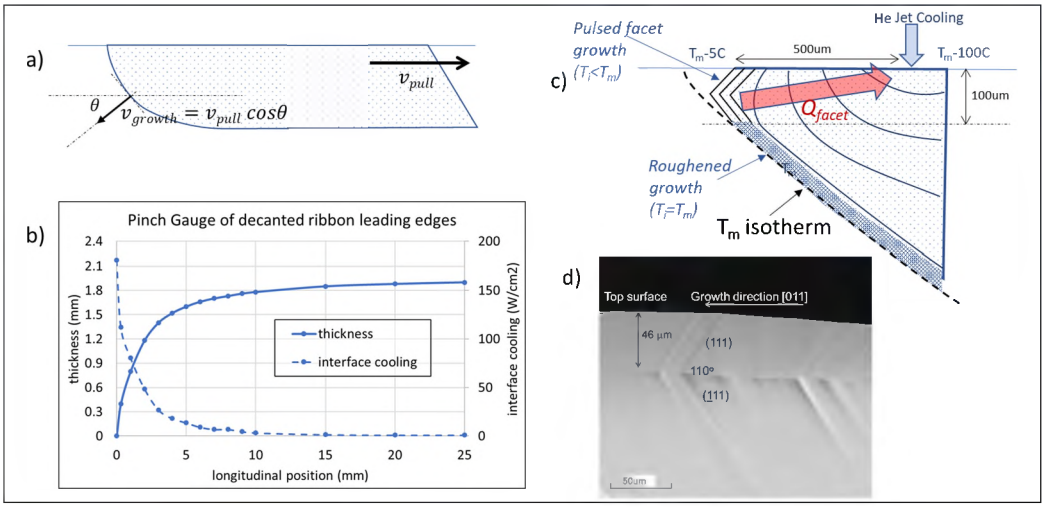

Figure 2: a) depiction of "decanted" ribbon leading edge. b) graph of leading-edge thickness measurement, along with calculated interface cooling heat flux. c) depiction of "pulsing" facet at leading edge. d) Antimony demarcation showing saccadic leading edge facet growth

The shape of the ribbon leading-edge can be measured by "decanting" a ribbon (i.e., halting the growth by turning off the cooling jet and rapidly pulling the ribbon out with minimal thinning. The shape of the leading-edge can then be measured by a thickness gauge, and the required latent heat removal and temperature gradient (on average) at the interface can be calculated (neglecting heat flow into the ribbon from the melt) as a function of position along the growth interface (z). Note that this measurement is too coarse to reveal evidence of the leading edge facet, which also gets rounded during the decanting process which still takes >20s to pull the ribbon out of the melt.

$$Q_{interface}(z) = L_f \rho v_{growth}(z) = L_f \rho v_{pull} cos\theta$$

$$\nabla T = \frac{Q_{interface}}{K}, \text{ where K is the conductivity of solid Si = .2W/cmK.}$$

Eq. 1

For the data shown in Figure 2, the ribbon was pulled at a steady speed of .5mm/s, then decanted at 5mm/s. One can see that the ribbon thickens rapidly to a thickness of ~2mm within a pull length of ~5mm. From eq. 1, the required heat removal at the tip interface must be close to 200W/cm^2, and the temperature gradient within the solid ~ 100K/mm. This heat removal (magnitude and extent) is commensurate with the He jet cooling but illustrates the extreme conditions necessary to support stable growth.

From Sb demarcation measurements [1, 7-9] as shown in Figure 2d (previously presented in [1]), one sees that although there is an average leading-edge growth rate at v_g of .5mm/s, the top 100um, in fact, pulses in facet layers ~10um thick with dual {111} facets intersecting at a "facet intersection line" (FIL). The Sb demarcation is due to differences in Sb concentration (resulting in differences in Wright etch [10] rate) and indicates a large difference in growth rate between the facet growth (which is kinetically inhibited) and the roughened growth in-between these facets. There is insufficient data to ascertain this growth rate difference directly from the Sb demarcation measurement itself, but let us for a moment assume that the fast and slow regions (wide and narrow stripes) are swept out in roughly equal time, such that $v_r/v_f \approx 10$ might be taken as an approximate figure. Estimating the widths of the bands to be w_f ~ 1um and w_r ~ 9um, and using the average growth speed, we obtain that the facet takes 10 ms to grow 1um, while the roughened growth takes 10 ms to grow 9um. Also from eq.1, the heat flux (i.e. latent heat out of interface) drops to 20W/cm^2 during the facet growth (due to the facet being kinetically inhibited), allowing the solid thermal gradient to intensify to provide the burst of cooling of ~400W/cm^2 during the roughened growth. This low value for facetted growth accords reasonably with other work on facet-inhibited silicon growth and may be taken as a validation that the v_r/v_f ratio is reasonable [11, 12].

3.2. Facet Formation (Limit Cycle Theory)

The pulsing nature of the leading-edge facet growth (slow/fast/slow/fast as described above) can be described by a limit cycle theory [1] (LCT), which, as a refresher, involves the following steps:

1. While the facet inhibits growth, the facet along with a small pool of melt cools below T_m until the kinetic roughening temperature is reached (~T_m-5C for Si) [12]. The extent of this pool is limited to the size of the facet, which from Sb demarcation is ~ 100um deep from the top surface (including both sides of the FIL. This is the slow growth phase.
2. A point on the FIL becomes morphologically unstable, and growth surges into the supercooled pool. Note that since Ste = Cp * $\Delta T/L_f$ = 0.36% at ΔT=5C (very small), the super-cooled pool can only support the unstable growth of a very thin needle or platelet before exhausting the available heat. From solutions to the transport equations for unstable growth into a supercooled melt [13-15] it is estimated that the tip of this surge has v_g >50cm/s with a R < 1um.
3. Although the tip of this platelet surge at the FIL continues to "sample" the {111} facet planes, new facets cannot form until the curvature is low enough that the size of a facet plane (flat to <1°) is large enough to withstand thermal fluctuations. The theory gives that this minimum radius of curvature is estimated to be ~ 1um and occurs when the surge reaches a length of ~ 10um, according with observations.

At this point, nascent facets have formed, spaced ~10um from the previous leading-edge facet, and the layer starts to fill in, or flow, with stable roughened growth. It should be emphasized that although this surge is morphologically unstable, it extends the crystal structure and orientation of the (100) ribbon, so that the newly formed facets are parallel to the original ones. That is, there is no independent nucleation of independent crystal grains.

3.3. Facet Flow Theory

Now let us newly consider how the facet completes in three dimensions. After initial platelet surge somewhere along the interface, two dimensions of growth go on simultaneously, with a) the platelet extending out along the leading edge while b) roughened growth works to fill the new volume above and below the 10 μm platelet. Taking the latter case first, once a new facet plane is established by these nascent facets at the end of the unstable surge platelet, the facet layer fills in (vertically) by propagating as roughened growth constrained between the old and new facet planes, depicted as a "wedge" in Figure 3b. This wedge consists of stable, roughened, growth with heat conducted through the cooled solid and drawing from the large thermal gradient therein. At the upper side of the wedge, the top surface expands as the roughened growth meets it, while at the lower side of the wedge the old facet roughens.

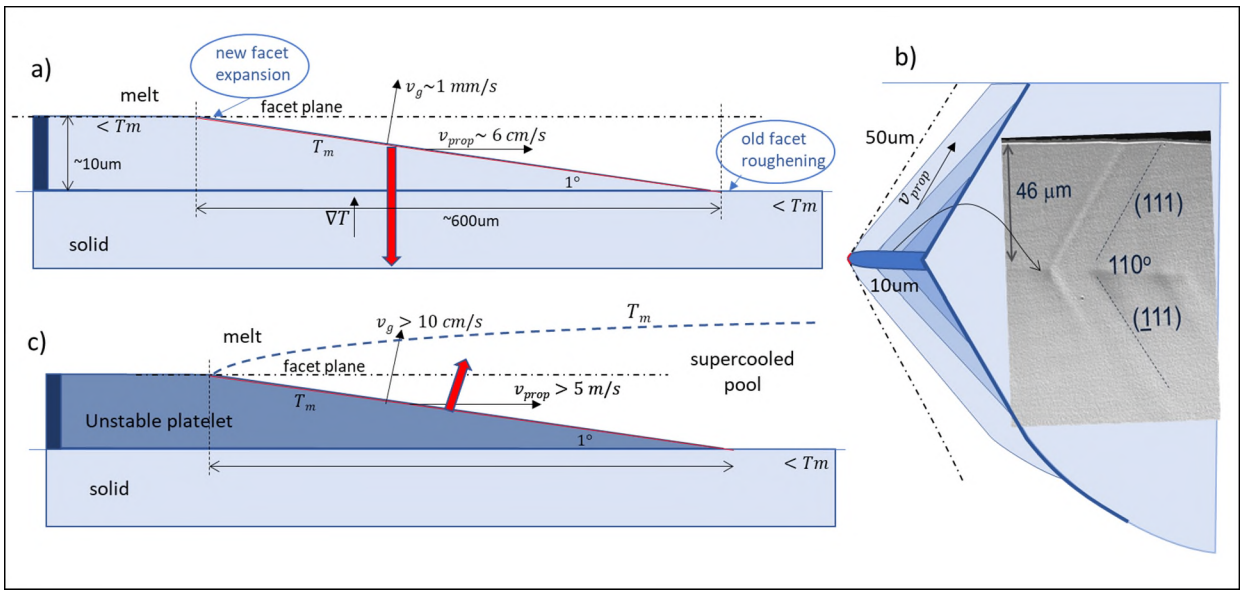

Figure 3: a) Top view depiction of steady-state facet flow. b) Cross-section depiction of vertical facet flow (stable layer "fill-in" from the unstable surge at the FIL, and Sb demarcation comparison. A difference in darkness above and below the FIL points to this as the likely location for the platelet surge. c) Top view depiction of horizontal unstable platelet propagation.

As new portions of the sub-cooled facet roughen, the new growth rapidly heats the interface to T_m, increasing the temperature gradient near the interface to support the rapid heat removal and growth rate. Using the same .5mm/s pull conditions as depicted in the previous section, this roughened growth rate v_g will be on the order of 1mm/s. The horizontal flow velocity of this propagation wedge, v_{prop}, depends on the wedge angle θ according to $v_{prop} = v_g/sin\theta$, limited only by θ.

The minimum wedge angle is the minimum mis-orientation angle (angle from a facet plane) such that the interface does not exhibit inhibited facet kinetics. This is, if the wedge angle were smaller than this minimum mis-orientation angle, it would behave as a facet, causing the wedge length to shrink (thereby increasing the wedge angle). For Si, Voronkov has estimated this angle to be ~1° (based on Cz data) [11, 16], resulting in a stable wedge propagation speed of ~6cm/s.

Figure 3b depicts how the facet layer fills in vertically from the unstable surge at the FIL. Using the facet layer thickness (facet line spacing) of 10um, the length of a steady state propagation wedge is $\frac{10um}{tan1^\circ} \sim 600um$. However, since the FIL is generally < 50um from the surface (from Sb demarcation), a complete propagating steady state wedge never forms, and instead the layer fills in with 1° wedges starting at the bottom of the FIL surge. Once the new expanding facet (at the top of the filled-in wedges) starts to flow upward the new facet is kinetically inhibited, so the heat removal becomes sensible, and the facet starts to cool < T_m. While these wedges fill in the layer, the unstable surge "fin" grows slowly due to the limited heat removal through its small cross-section. This is consistent with the apparent Sb demarcation of the thin surges at the FIL (the darkened FIL line shown in Figure 3b).

In the horizontal direction, a similar facet flow phenomenon occurs. Figs. 3a and 3c illustrate competing theories for how the horizontal flow may occur. From the observed continuity of facet

lines across the width of the ribbon (>10cm long), it is believed that this horizontal facet flow occurs at the unstable platelet surge phase of the faceted layer growth, as depicted in Figure 3c. Here, the wedge grows as a microscopic platelet via cooling from the super-cooled pool in front of the FIL across the ribbon. This unstable growth would still be confined to the newly formed facets that are now extending as narrow lines of facets across the ribbon width. Since this growth is extremely fast (estimated to be > 10cm/s), the surge propagation speed across the ribbon would be > 1m/s, making the facet initiation across the ribbon a virtually synchronous event. This surge platelet (with nascent facets) at the FIL running across the width of the ribbon would then fill-in vertically with stable growth via heat conduction through the solid as described previously. Note that, if the horizontal facet flow were to occur during the stable growth fill-in, it would be much slower, taking ~ 10cm/(6cm/s) ≈ 1.6s to flow across the ribbon. If that were the case, the facet would "fall-back" (as the ribbon is pulled at .5mm/s) into the jet cooling curve by ~1mm, resulting in multiple facet layers being initiated along the width (counter to observation). In addition to explaining the observation of continuous facet lines across the ribbon, the "synchronous" flow of the FIL surge platelet across the ribbon also explains the observed Sb demarcation of the surge platelet at any location across the ribbon.

3.4. Side Effects

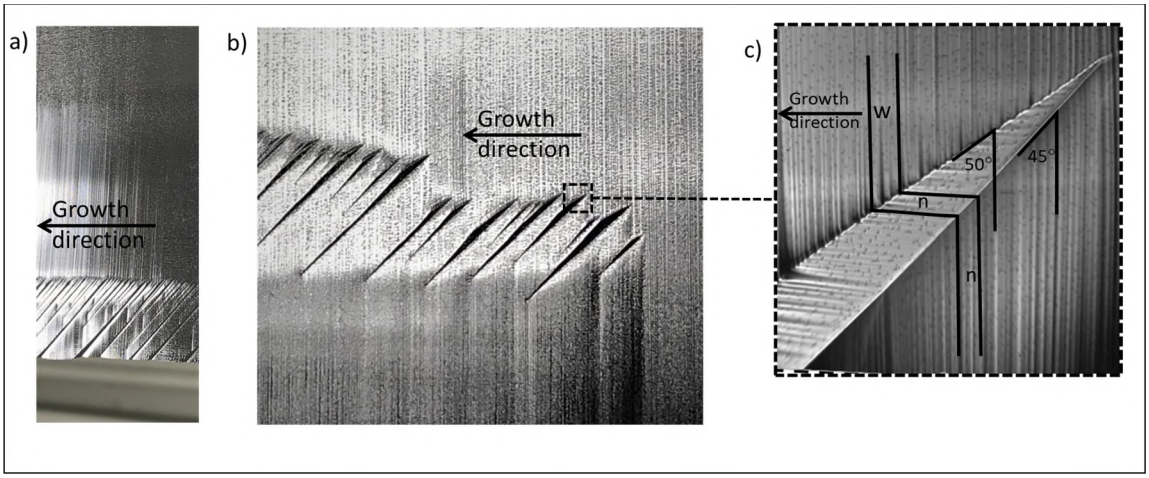

Figure 4: a) Photo of Side Effects as seen on the surface of a ribbon at the ribbon edge. b) Photo of Internal Side Effects occurring inboard from the edges. c) Micrograph detailing the anatomy of a SE or ISE, showing the trace of 6 facet lines, indicating where they are wide (w) and narrow (n), and the resulting mitered angles. The facet flow direction moves from the top of each image to the bottom.

"Side Effects" (SE) is a 3D manifestation of facet layer growth that occurs where the gas jet cooling drops off at the edge of a ribbon, or occasionally within the ribbon if there is a severe non-uniformity of gas cooling (which are referred to as "Internal Side Effects" (ISE)). Either SEs or ISEs are the result of the "perpendicular" {111} facet planes being sampled causing perpendicular facet lines (as seen from the top surface) to form. These appear as microscopic "mitered" patterns on the surface of the ribbon, as shown in Figure 4c. It should be emphasized that within these patterns the underlying single crystal structure is maintained.

All SEs and ISEs share a common anatomy: 1- facet lines are continuous throughout the mitered structure, i.e., facet lines neither start nor end; 2- at the start of a SE, the inner mitered joint forms an angle of ~50-55° with respect to the original facet lines while the outer joint is at 45°, creating an initial wedge of angle ~5-10°. Consistent with this, one finds that the facet layer widths are narrower within and outboard of the SE wedge (as compared with the center portion of the ribbon).

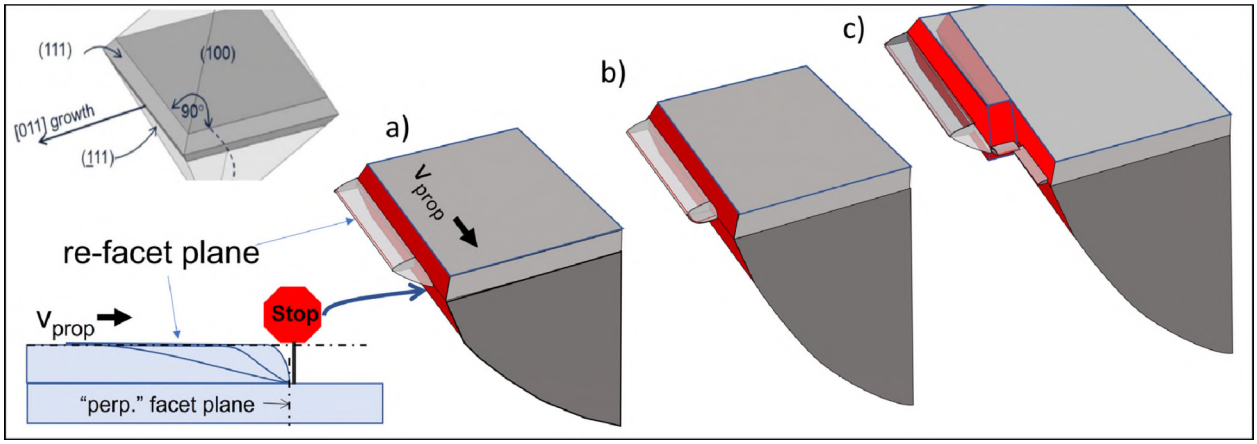

Figure 5: Depiction of Side Facet formation: a) facet layer flow gets to the edge of the jet cooling and stops. b) as this layer "squares off", it samples the perpendicular facet planes. c) independent facets form, creating the perpendicular facet layers of the SE geometry and later nucleating their own growth platelets.

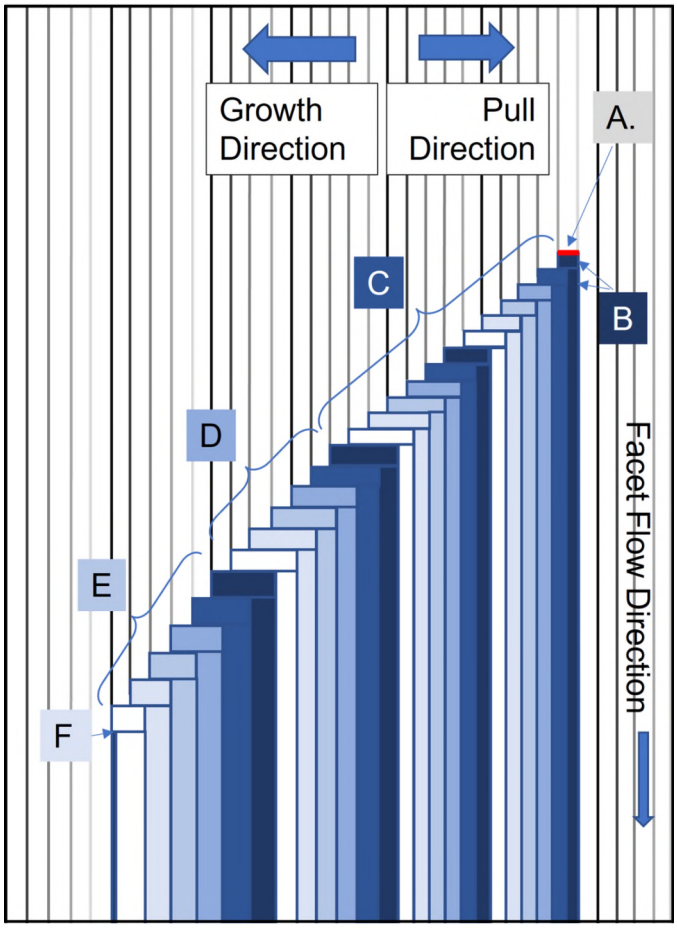

Figure 6: Internal Side Effect formation. The initiation, expansion and extinction of an internal side effect proceeds as follows: A. Facets flowing from the top hit the "STOP" sign of Fig. 5a and a side facet forms. Beyond the side facet, extra time allows extra supercooling to build up. The next platelet

layer flows in from the top. At the side facet, the platelet makes it around the corner and initiates layer B as it heads to the edge of the ribbon, but at reduced width. New layers continue to move around the corner, where narrower widths outboard of the side facet cause the ISE to widen at 5-10 deg based on the ratio of the layer widths from the ISE to the center. In many cases, ISE expansion stops as the ISE moves away from its initiation point, as in section D. In section E, the ISE shrinks as the corner layers grow wider than the layers flowing from the center until at F the ISE disappears entirely.

These SE features can be explained using Facet Flow Theory (Figure 5): as a new layer (unstable platelet growth) flows along the width of the ribbon leading edge, it eventually encounters a region where, for one of various reasons, (e.g. a local reduction in cooling), the propagating platelet wedge can no longer advance. This results in the propagation wedge "squaring off", eventually sampling the "perpendicular" {111} planes and forming nascent side facets at 90 degrees to the leading edge. These new facet layers then fill in with stable growth, resulting in the mitered appearance of facet lines as seen from the top.

At the location where these SE's form, new layers coming from the center will also stop at the perpendicular facet. As more layers pile up and the ribbon gets pulled further, the stunted side area gets pulled closer to the peak cooling. The supercooling in the melt increases and eventually the new perpendicular and outer facets initiate their own surge layers in both directions from the interior corner.

In Fig. 6, the complete life cycle of an internal side effect is depicted. Actual side effects tend to extend through 100's or 1000's of layers, but for clarity a 25 layer example is shown (~250 microns). Initially, the complete facets are arrested at a given point and form a side facet. The section of growth front beyond the side facet continues to build up supercooling in the ~20 ms before the next facet line platelet arrives. Close examination suggests that the very next layer is continuous with a perpendicular layer and a continuation of growth out to the end of the ribbon. These layers formed around the corner from the central growth front are observed to have narrower width than the main layers. The fact that the outer angle is always 45 degrees strongly indicates a crystallographic

influence. The side effect layers growing perpendicular to the growth front and parallel out towards the edge seem to be nucleated simultaneously in the inner corner and with identical layer width. This identical layer width is what maintains the 45 degree angle. The observed 50-55° inner angle (or 5-10° opening angle for the ISE) arises from the difference in thickness between the central layers and the side effect layers. One can infer that the ratio of layer thicknesses must be around tan(52°) = 1.3 = 4:3. As the smaller side effect layers pile up and the length of the perpendicular facet grows, the outer edge of the growth front falls further and further behind the central growth front, pulling that section closer to the most intense cooling and driving up the thermal gradients. The inner and outer angles of the ISE have the effect of moving the side effect away from its nucleation point, potentially changing the thermal conditions involved. In section D of Fig. 6, the thickness of the layers of the main section and the ISE go 1:1 and the side effect keeps a constant size. Past this, in section E, the ISE layer thicknesses increase further and the outer layers start catching up to the main section of the leading edge until the side effect is extinguished and normal growth resumes (labeled "F"). Note that, while the side effect layer thicknesses in Fig. 6 increase from C to D to E, the two perpendicular parts of the side facet maintain the same thickness, enforcing the 45 degree outer angle.

In at least two cases, these SE structures can repeat in a ribbon, forming a "feathering" visual effect as seen in Figure 5 (a,b). This can be due either to a stagnant hot spot along the growth front nucleating a new ISE once the old one moves far enough away, or to misalignment of the growth front with the plane of the cooling jet, which will cause periodic ISEs at a spacing predictable from the misalignment. Although the presence of SEs or ISEs does not affect the single crystal quality of the ribbon, it can affect the local topography of the ribbon, detracting from the wafer Total Thickness Variation (TTV). It is therefore important to design the gas cooling jet with a high degree of uniformity to prevent ISEs from forming. The FSM furnace is also designed such that the ribbon is

sufficiently wide to allow the edge SEs to be laser trimmed as the ribbon emerges from the furnace while maintaining the specified wafer dimensions.

4. Thickness Control

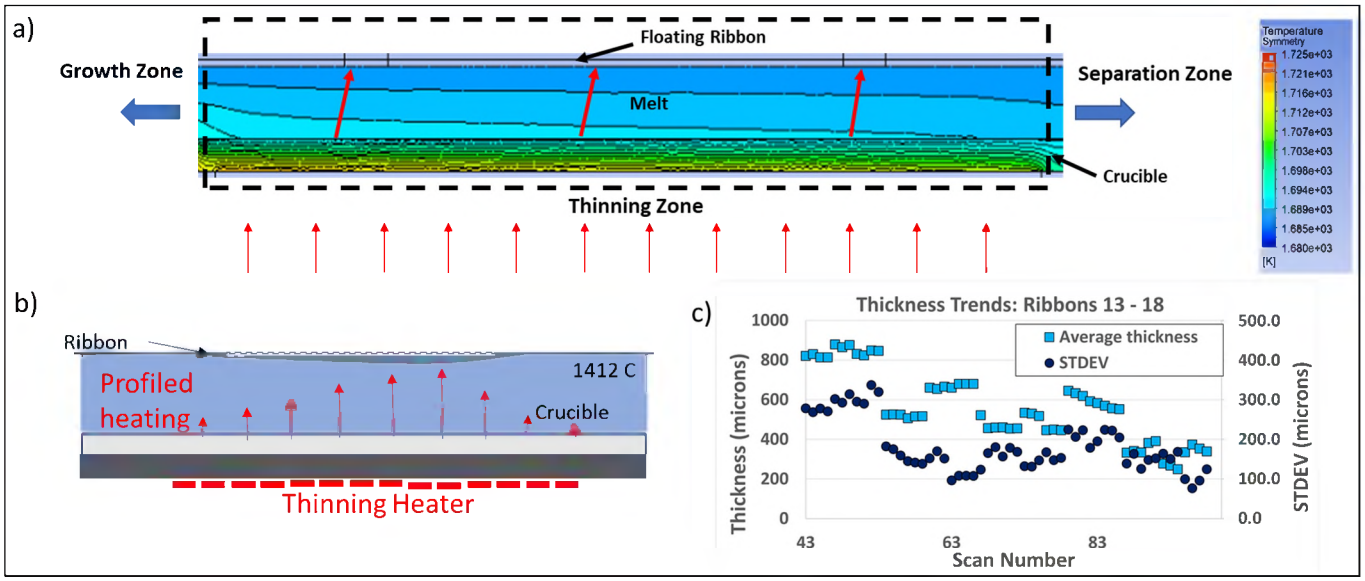

Figure 7: a) Thermal model showing the heat flux going into the floating ribbon in the thinning zone. b) Method to modulate thickness and achieve uniformity using profiled heating from the bottom. c) Experimental data showing iterative improvement in thickness average and uniformity over multiple samples

As discussed in Section 3, the steep angle of the facets that form at the leading edge pose the requirement of large cooling flux to sustain growth. In principle, if this large cooling flux is provided within an extremely narrow length span (~500 um), it would be possible to sustain growth of ribbons close to the thickness target (~200 um). However, in practice, this cooling flux profile is diffuse, extending over several millimeters, resulting in a much thicker ribbon (in the range of 1-2 mm). Although the growth jets are designed to grow uniform material thickness in the transverse direction, it tends to be non-uniform due to non-idealities in equipment, gas interactions and melt convection effects. The floating nature of the ribbon in the FSM process presents a unique

opportunity to manipulate the ribbon thickness post growth and before it separates from the endwall of the crucible, see Figure 7a. We have implemented this thickness control (Figure 7b) using profiled heat control that can be generated as shown by multiple segmented heaters controlled appropriately to yield a uniformly thin ribbon at the target value. Since the ribbon's thickness profile is measured at the exit of the furnace, a modeled based thinning algorithm (MBTA) is needed to determine the correct thinning settings to attain the target uniformity and thinness. This MBTA utilizes "response function" profiles of the profiled heat channels that are based on models and experimental data. A few iterations may be required to achieve a final thinness and uniformity. While we have on-going efforts to optimize this scheme to be more effective, Figure 7c shows an example of experimental demonstration where the average thickness is iteratively lowered, and uniformity improved over multiple samples. Each data point in Fig. 7c represents the average or standard deviation of a ~100 point thickness profile across one lateral cross-section of the ribbon. These scans are taken at regular intervals across six consecutive ribbon attempts within a run, showing improvements in thickness and TTV both within ribbons (using feedback loops) and between ribbons. At the right end of the graph, thicknesses sit in a range of ~350 microns (left axis) while standard deviations average around 100 microns (right axis).

5. Characterization

The single crystal silicon produced by the Floating Silicon Method has a unique and advantageous profile of impurities and defects. The process uses a fused quartz crucible (as do other single crystal processes) because the dissolution of the crucible into the silicon over time does not lead to precipitate formation. With high purity graphite or silicon nitride crucibles, the incorporation of carbon and nitrogen into the melt tends to lead to saturation and precipitation of carbide and nitride particles, respectively, at the colder points of the melt. These particles have a strong

likelihood to disrupt the propagation of the single crystal structure at the crystal growth interface. Oxygen, on the other hand, does not precipitate in the melt, but instead either incorporates evenly into the crystal or evaporates off the free melt surface as SiO molecules. Factors like convection and the ratio of free melt surface to wetted crucible surface determine the equilibrium oxygen concentration that is incorporated into the growing crystal at a greater than 1:1 impurity segregation ratio.

In FSM material, we have measured varying levels of oxygen depending on the growth conditions. It is possible to grow material with high levels of oxygen (20-25 parts per million atomic or ppma), but we generally target lower levels that are better suited for high efficiency solar cells, see Table A.

Table A: Interstitial and Precipitated Oxygen and Substitutional Carbon concentrations as measured by Fourier Transform Infrared (FTIR) spectroscopy.

FTIR Data	AS GROWN		AFTER OXIDE GROWTH	Calculated	
Sample ID	**[Cs] (avg)** (ppma)	**[Oi] (avg)** (ppma)	**[Oi] (avg)** (ppma)	**Precipitated Oxygen** % of AG	**Precipitated Oxygen** ppma
LE 20-8-AG		7.1	3.4	52.1%	3.7
LE 21-14-AG		6.2	2.9	53.2%	3.3
LE 21-17-1-AG		10.3	2.4	76.7%	7.9
LE 21-17-2-AG		7.3	3.5	52.1%	3.8
LE 24-9-52-AG	1.7	26	13.1	49.6%	12.9
LE Average		11.4	5.1	56.7%	6.3
CZ Comparison	0.9	23	6.9	70.0%	16.1

In material from 3 different runs, we see a fairly wide range of interstitial oxygen concentrations, These ranges are traceable back to the growth conditions, and specifically the ratio of free melt surface area, A_{fm} to wetted crucible surface area, A_{wc}, where smaller A_{fm}/A_{wc} correlates to lower [O_i].

Unlike oxygen, carbon typically incorporates into the melt in quartz crucible processes (CZ, multi, etc.) by vapor-phase transport from areas in the furnace where SiO reacts with exposed carbon sources. Careful routing of exhaust gas allows the FSM material to control carbon concentrations to a range from 0.5 – 2.0 ppma. Oxygen incorporates into the silicon lattice at the crystal growth front into interstitial positions. The distribution of oxygen in a finished solar cell (interstitial or precipitated) depends on the cooling profile of the crystal growth, the concentration of nucleation aides like carbon and nitrogen, and the subsequent thermal processes that the wafer sees. The cooling process for FSM material is much faster than for CZ silicon, see Figure 8.

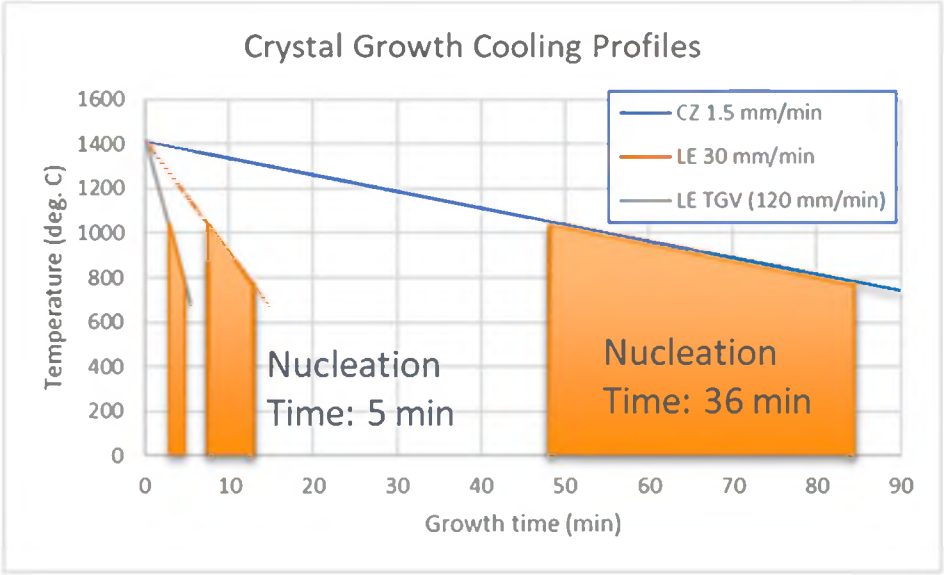

Figure 8: Cooling profiles and associated nucleation times for CZ pulled at 1.5mm/min and Leading Edge crystal growth at two pull speeds.

In state of the art solar cells, minority carrier lifetimes can be influenced by oxygen in two ways. First, interstitial oxygen at high concentrations (>7E17 atoms/cm^3) can complex with boron at resistivities < 2 ohm-cm. Recent trends towards gallium doping and n-type have decreased these concerns. Second, precipitated oxygen acts as an internal gettering site for mobile metals and is usually the limiting factor for high end solar cells. Nucleation of oxygen precipitate nuclei is considered to occur primarily between 1050 °C and 750 °C, during the cool-down phase of crystal

growth.[17] Figure 8 presents a comparison of the cooling profiles for FSM at two growth speeds and Cz growth at the industry standard pull speed. The time spent in the precipitate nucleation zone for even the slowest case of FSM is ~15% of the CZ process, leading to fewer nuclei. To investigate the effects of density of nuclei on precipitation, a comparison was done on precipitation behavior between CZ and FSM material. Wafer samples from both processes were put through 4h of 800 °C to stabilize nuclei and 16h of 1000 °C to grow precipitates in a box furnace. The results are also summarized in Table 1, where an average of 56% of the FSM oxygen has precipitated (independent of the starting concentration) compared with 70% of the CZ oxygen. 16h at 1000 °C is extreme compared with typical solar cell processes, but even a standard emitter diffusion causes the growth of oxide precipitates to a point where they become permanent internal gettering sites for transition metals. As previously mentioned, the ultimate concentration of the resulting metal-decorated oxygen precipitates (typically called bulk micro-defects or BMDs) ends up being the limiting factor for both CZ lifetime and cell efficiency. [18] In our simulations of 140 micron PERC-type solar cells on p-type wafers, reduction of BMD density from 10^9 defects/cm^3 to 10^8 defects/cm^3 resulted in a solar cell efficiency enhancement from 21.0% to 22.9%. The lower concentration of internal gettering centers is critical for FSM, since its high surface area to volume ratio makes it prone to metal contamination. In order to succeed, FSM requires a high efficacy of external gettering. The net benefit is plain to see in comparisons of final device MCL with as-grown MCL. We measured bulk lifetimes from surface-passivated samples that were (A) in the as-grown state and (B) put through the entire PERC cell process and then stripped back to bare wafers. From an average of 28 samples put through the cell process and measured on a Sinton lifetime tester at 1E15/cm^3, the final lifetime (B) averaged 68 times the initial lifetime of (A).

6. Conclusions

In this paper, we have described FSM process and how it can produce low-cost, high efficiency wafers in the final form factor as drop-in replacement for the incumbent Cz technology. The pulsing nature of the leading-edge facet growth is heuristically described by a Limit Cycle Theory, alternating between slow facet growth and fast roughening growth, based on physical observations, heat-flux requirements, and kinetic limitations. A 3D Facet Flow Theory is proposed that describes how the facet layer fills in both vertical and horizontal directions, consistent with the observation of continuous facet lines across the ribbon width, along with the breakdown of relevant timescales. The Facet Flow Theory is further applied to explain the formation of the internal single crystal defect, ISE, and its anatomy is presented. The design and analysis of cooling jets and stabilization heat used in the FSM process to promote the limit cycle growth at the leading edge while maintaining morphological stability is discussed. The need to melt back the thick ribbon, due to the nature of cooling jets and faceted growth, to a target thickness is explained and an experimental demonstration of such thickness control is shown. Impurity characterization measurements showing lower than Cz interstitial Oxygen concentration as well as low concentrations of metal-decorated oxygen precipitates, due to the unique cooling rates of FSM process, emphasize the high lifetime of FSM substrates and potential high cell efficiencies.

Acknowledgements

This work has been supported by the US Dept of Energy, EERE division under grants DE-EE0008971 and DE-EE0008132, and by the National Science Foundation Small Business Incubator Program under NSF SBIR 2024523

References

[1] P. Kellerman, B. Kernan, B. Helenbrook, D. Sun, F. Sinclair, F. Carlson, "Floating Silicon Method single crystal ribbon- observations and proposed limit cycle theory" *J Cryst. Growth* 451 (2016) 174-180.

[2] https://leadingedgetech.io/solar-manufacturing-technology/

[3] William Shockley, "Process for Growing Single Crystals", US Patent 3,031,275A (1962).

[4] C. Bleil, "A new method for growing crystal ribbons", J. Cryst. Growth 5 (2) (1969) 99–104.

[5] H. Bates, D. Jewett, "Low angle silicon sheet growth: a review of progress, Problems and Promise", in: Flat-Plate Solar Array Proj. Res. Forum on the High-Speed Growth and Characterization of Crystals for Solar Cells vol. 1 (1984), pp. 297–307.

[6] B. Kudo, Improvements in the horizontal ribbon growth technique for single crystal silicon, J. Cryst. Growth 50 (1) (1980) 247–259.

[7] A. Murgai, H. C. Gatos, and A. F. Witt, "Quantitative Analysis of Microsegregation in Silicon Grown by the Czochralski Method," *J. Electrochem. Soc.* 123 (2) (1976) 224–229.

[8] A. Murgai, H. C. Gatos, and W. A. Westdorp, "Effect of Microscopic Growth Rate on Oxygen Microsegregation and Swirl Defect Distribution in Czochralski-Grown Silicon.," *J. Electrochem. Soc.*, 126 (12) (1979) 2240 – 2245.

[9] A. F. Witt, M. Lichtensteiger, and H. C. Gatos, "Application of Interface Demarcation to the Study of Facet Growth and Segregation: Germanium," *J Electrochem Soc USA* 121 (6) (1974) 787 – 90.

[10] M.W. Jenkins, "A New Preferential Etch for Defects in Silicon Crystal", J. Electrochem. Soc. 124 (1977) 757-759.

[11] O. Weinstein and S. Brandon, "Dynamics of partially faceted melt/crystal interfaces I: computational approach and single step–source calculations", *J. Cryst. Growth* 268 (1) (2004) 299–319.

[12] W. Miller, *J. Cryst. Growth* 325 (2011) 101-103.

[13] M. E. Glicksman, *Principles of Solidification*, Springer Science+ Business Media, 2011.

[14] G.P. Ivantsov, *Dokl. Akad. Nauk.,* USSR, 558 (1947) 567.

[15] G. Horvay and J. Cahn, "Dendritic and spheroidal growth," *Acta Metall.*, vol. 9, no. 7, pp. 695–705, 1961.

[16] V.V. Voronkov, in: A.A. Chernov (Ed.), "Crystals Grown, Properties, and Applications", Modern Theory of Crystal Growth 9 Springer (1983).

[17] J. Osaka, N. Inoue, K. Wada, "Homogeneous nucleation of oxide precipitates in Czochralski-grown silicon", *Applied Physics Letters* **36** (4), 1980

[18] J. D. Murphy, K. Bothe, M. Olmo, V. V. Voronkov, and R. J. Falster, "The effect of oxide precipitates on minority carrier lifetime in p-type silicon," *JOURNAL OF APPLIED PHYSICS* **110**, 053713, 2011